Accepted Manuscript

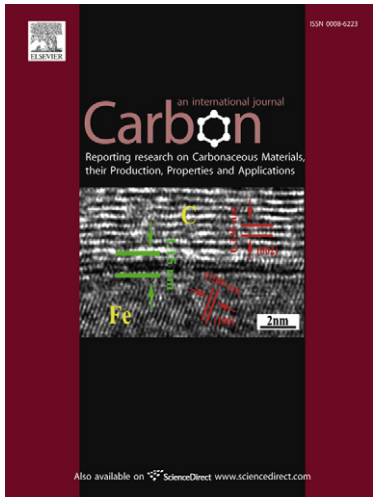

Functionalization of Single Walled Carbon Nanotubes with Optically Switchable Spiropyrans

Elisa Del Canto, Kevin Flavin, Manuel Natali, Tatiana Perova, Silvia Giordani

PII: S0008-6223(10)00263-0
DOI: 10.1016/j.carbon.2010.04.012
Reference: CARBON 5849

To appear in: *Carbon*

Received Date: 27 October 2009
Accepted Date: 9 April 2010

Please cite this article as: Canto, E.D., Flavin, K., Natali, M., Perova, T., Giordani, S., Functionalization of Single Walled Carbon Nanotubes with Optically Switchable Spiropyrans, *Carbon* (2010), doi: 10.1016/j.carbon.2010.04.012

Functionalization of Single Walled Carbon Nanotubes with Optically Switchable Spiropyrans

Elisa Del Canto[a], **Kevin Flavin**[a], **Manuel Natali**[a], **Tatiana Perova**[b] **and Silvia Giordani**[a1]

a) School of Chemistry / CRANN, University of Dublin Trinity College, Dublin 2, Ireland.

b) Department of Electronic & Electrical Engineering, University of Dublin Trinity College, Dublin 2, Ireland.

[1] Corresponding author. Fax: +353 16712826

E-mail address: giordans@tcd.ie (S. Giordani)

Abstract

The design, synthesis and complete characterization of a smart material composed of single-walled nanotubes functionalized with spiropyran-based photo switchable molecules are reported. The chemical complexity of the system requires the use of a range of complementary techniques in order to provide a complete picture of the composition and performance of the nanomaterial. Thermal gravimetric analysis ensured both the high degree of chemical functionalization and the presence of molecular switches in the nanotube sample; micro-Raman indirectly confirmed the successful oxidation of the tubes, FT-IR proved the nature of the functional groups introduced based on their characteristic stretching vibrations and atomic force microscopy demonstrated nanotube lengths of approximately 600 nm. UV-Vis-NIR absorption spectroscopy was used to evaluate the photoresponsive behaviour of the nanomaterial, and the intensity of the absorption band at 556 nm could be modulated by light-induced reversible conversion of the spiropyran molecules attached to the SWCNT from the spiro close conformation to the merocyanine open form. We were also able to provide the first example of a continuous solution based on-off switching in a spiropyran-nanotube material.

1. Introduction

Modern technology is constantly pushing towards smaller and lighter devices, and future applications will require materials that respond to their environment in a manner that suggests a degree of "intelligence". In this context, robust molecular sensors that can detect changes in their environment with a high degree of selectivity and sensitivity represent important building blocks of target-oriented smart materials. In order to reduce manufacturing costs and to increase versatility, a modular system comprising a scaffolding with appropriate physical properties, and molecular building blocks that can be readily interchanged to meet specific performance parameters, offer considerable promise that may lead to nanosized devices that are truly multi-tasking and target-oriented.

Single walled carbon nanotubes (SWCNTs) [1, 2] were chosen as the scaffolding due to their remarkable mechanical, thermal, electronic [3-5] and optical properties [6] in addition to their biocompatibility. They are also suitable as a foundation for modular materials as it has been demonstrated, in recent years, how SWCNTs can be solubilized and decorated with a range of molecules via both covalent and also by non-covalent means [7, 8].

A remarkable class of photochromic molecular switches, known as spiropyrans (SPs), were selected for conjugation to the SWCNTs scaffold. These were specifically chosen as they have shown the ability to undergo reversible conformational transformations in response to light [9], pH [10], change in the environment such as solvent polarity and various ligands [11,12]. The tremendous versatility of this class of compounds and in particular their fast stimuli responsiveness and high sensitivities [13] makes them legitimate candidates for applications in nanoelectronics. Among the class of molecular

switches, spiropyrans have been probably the most extensively studied over the past several decades owing to the profitable applications they could be used for. Already in his early work Hirshberg envisaged the suitability of such compounds as photochemical erasable memory [14]. Furthermore, optical molecular switches have attracted much attention as a result of their potential use in optical data storage and digital processing [9], sensing [15] and photoregenerable surface modifications [13]. The preparation of integrated nanomaterials where switchable molecular units are coupled to SWCNTs has received some interest recently [16-19], with Haddon and co-workers initially demonstrating the possibility of photo-inducing electronic transitions in semiconducting nanotubes [16].

Materials of this type are likely to display considerable chemical and structural complexity and it is therefore imperative that we develop comprehensive protocols for reliable characterization in parallel with the actual design and synthesis of the materials themselves. An array of fundamentally different techniques such as thermal gravimetric analysis, FT-IR, micro-Raman, UV-Vis-NIR absorption spectroscopy and atomic force microscopy were utilized, in order to provide a complete picture of the composition and performance of a modular smart material composed of single-walled nanotubes (acting as the scaffolding) functionalized with spiropyran-based photo switchable molecules (which provide the 'intelligence'). In addition, we also demonstrate the first example of a continuous solution based on-off switching in such a system.

2. Experimental Methods

2.1 Materials. SWCNTs produced by the HiPco technique were purchased from Unidym®, Inc. (Lot no. R0546). Reagents and solvents were purchased as reagent-grade from Fisher Scientific Ireland Ltd, or Sigma-Aldrich Ireland and used without further purification.

2.2 Preparation of o-SWCNT (1). HiPco pristine SWCNTs (Unidym® lot R0546) were weighted (100 mg) and dispersed in 100 mL aqueous solution of HNO_3 (2.6 M). The dispersion was stirred under reflux at 100 °C for 48 h. After cooling down to room temperature the dispersion was filtered through a Millipore system (on a 0.2 μm Isopore filter) and the black solid powder collected on the filter was rinsed with distilled water (until the pH value of the filtrate was neutral) and dried overnight at 60 °C under vacuum. The purified nanotubes were subsequently dispersed in distilled water, sonicated for 10 min and treated with 100 mL of piranha solution ($H_2SO_{4\ conc} \cdot H_2O_2$ (30%) at a 4:1 ratio) and the mixture was stirred at 35 °C for one hour. After cooling down to room temperature the mixture was diluted with ice and filtered through a Millipore system (on a 0.2 μm Isopore filter) and the residue rinsed with distilled water (~ 500 mL) until the pH of the filtrate was neutral. After drying at 60 °C under vacuum overnight 78 mg of oxidized and shortened o-SWCNTs (**1**) were obtained. **FT-IR** υ (cm^{-1}): 3004, 2900, 2836 (C-H), 1740, 1714 (C=O), 1603, 1492, 1431 (C=C), 1384, 1310 (C-C), 1283, 1207, 1156 (C-O-C).

2.3 Preparation of tert-Butyl 3-(2-(2-(3-aminopropoxy)ethoxy) ethoxy)propylcarbamate (2). A solution of 4,7,10-trioxa-1,13-tridecanediamine (17.53

mL, 2 equiv, 80.0 mmol) in 60 mL of dichloromethane (DCM) was added dropwise to a solution of tert-butoxycarbonyl anhydride (Boc_2O) (8.74 g, 1 equiv, 40.0 mmol) in 60 mL of DCM over a three and a half hour period at 0 °C. The solution was then stirred at room temperature for 24 h. The solvent was evaporated and the residue was added to distilled water (~ 100 mL). The bis-Boc protected derivative, insoluble in water, appeared as a white precipitate. The latter was removed by filtration on celite. The water was extracted 5 times with dichloromethane (15 mL). The organic phases were unified and dried with Na_2SO_4 anhydrous. After solvent evaporation under reduced pressure the product (**2**) was obtained as yellowish oil. **Yield** 68%. R_f = 0.8 (CH_2Cl_2·MeOH 9:1). **^{1}H-NMR** (400 MHz, $CDCl_3$): δ = 1.43 (s, 9H, Boc), 1.71-1.85 (m, 4H, CH_2), 2.90 (t, 2H, J= 6.0 Hz, C$H_2$$NH_2$), 3.23 (d, 2H, J= 5.5 Hz, CH_2NH), 3.35-3.41 (m, 2H, CH_2), 3.53-3.64 (m, 10H, CH_2), 5.16 (bs, 1H, NH). **^{13}C-NMR** (100 MHz, $CDCl_3$): δ = 28.0 ($3CH_3$), 29.2 ($CH_2CH_2NH_2$), 31.3 (CH_2CH_2NH), 38.0 (CH_2NH), 39.1 (CH_2NH_2), 69.2 (CH_2), 69.6 (CH_2), 69.7 (CH_2), 70.0 (CH_2), 70.1 (CH_2), 74.1 (CH_2), 78.5 (C Boc), 155.7 (COO). **FT-IR** υ (cm^{-1}): 3351 (NH), 2929, 2866 (C-H), 1693 (C=O), 1517 (N-H), 1364 (C-tBut), 1249 (CO-O-C), 1105 (C-O-C). **HRMS (*m/z* -ES):** Found: 321.24 (M+ H^+, $C_{15}H_{32}N_2O_5$ Requires: 320.43).

2.4 Preparation of f-SWCNTs (3). o-SWCNTs (**1**) were weighted (70 mg) and dispersed in approximately 50 mL of dimethylformamide (DMF) by sonication in a water bath for 10 min. N-hydroxysuccinimide (NHS) (30 mg in 5 mL of DMF) was added to the dispersed o-SWCNTs (**1**) and the dispersion was sonicated for another 10 min. 1-Ethyl-3-(3-dimethylaminopropyl)carbodiimide hydrochloride (EDC·HCl) (46 mg in 5mL of DMF), was added to the dispersion of o-SWCNTs and the sonication continued for an

additional 10 min. The reaction mixture was stirred at room temperature for 30 min and tert-butyl 2-(2-(2-aminoethoxy)ethoxy)ethylcarbamate (**2**) (138 mg in 25.5 mL of DMF) was added. Pyridine (5.4 mL) was added and the reaction mixture was stirred at room temperature for 3 days under N_2. The functionalized SWCNTs (**3**) were collected as a black precipitate and filtered twice through Millipore system (on a 0.2 μm fluoropore FG filter). The black solid collected on the filter was dissolved in DMF, sonicated for 10 min and filtered again on a new 0.2 μm fluoropore FG filter. The product was washed with increasing polarity solvents toluene, diethyl ether, dichloromethane and methanol to remove the excess of non-reacted products. The black solid was dried under vacuum overnight to afford 76 mg of f-SWCNTs (**3**). **FT-IR** υ (cm^{-1}): 3252 (NH), 2915, 2845, 2603 (C-H), 1739 (C=O), 1570, 1522 (N-H), 1435 (C-tBu), 1150 (C-O-C).

2.5 Preparation of SP (4)

The spiropyran 4-(3',3'-dimethyl-6-nitrospiro[chromene-2,2'-indoline]-1'-yl)butanoic acid (**4**) was synthesized according to the literature procedure previously reported.[20]

2.6 Preparation of f-SWCNTs (5). A 66 mg quantity of the previously obtained f-SWCNTs (**3**) was dispersed in 25 mL of DMF and sonicated in sonic bath for 20 min. A 4.5 mL aliquot of trifluoroacetic acid (TFA) was added and the mixture was stirred at room temperature for 9 h. The black product was filtered through a Millipore system (on a 0.2 μm fluoropore FG filter) and washed in order with pyridine, dimethylformamide, toluene, diethyl ether, dichloromethane and methanol. The black solid was dried under vacuum to afford 57.8 mg of f-SWCNT. **FT-IR** υ (cm^{-1}): 3261 (NH), 3061, 2866 (C-H),

1737, 1651 (NH-CO), 1651, 1571 (N-H), 1431 (C-C), 1054 (C-O-C). Solutions of spiropyran (7 mg in 1 mL), NHS (2.2 mg in 1 mL) and EDC·HCl (3.3 mg in 1 mL) in DMF were added sequentially. The solution was stirred at room temperature for 10 minutes in order to activate the carboxylic groups and the sonicated deBoc f-SWCNTs (40 mg in 60 mL of DMF) and pyridine (1.2 mL) were added. The reaction mixture was stirred at room temperature for 2 days under a nitrogen atmosphere. The product was collected as a black precipitate and was filtered through a Millipore system (on a 0.2 μm fluoropore FG filter). The residue was collected, dissolved in 10 mL of DMF and sonicated for 10 minutes. The f-SWCNTs (**5**) were refiltered through Millipore system (on a 0.2 μm fluoropore FG filter) and washed with toluene, diethyl ether, dichloromethane and methanol to completely remove any unreacted products. The black solid was dried under vacuum overnight to afford 36 mg of spiropyran f-SWCNT (**5**). **FT-IR** υ (cm^{-1}): 3265 (N-H), 2908, 2844 (C-H), 1732 (NH-CO), 1577, 1362 (NO_2), 1478 (C-C), 1520 (C=C), 1217, 1114, 1091 (C-O-C).

2.7 Characterization. All TGA analyses were performed on a PerkinElmer Thermogravimetric Analyzer Pyris 1 TGA. The method used for performing TGA measurements both in air and nitrogen is as follows: 5 minute isothermal step at 30 °C (to equilibrate the sample); heat from 30 °C to 100 °C at a rate of 10 °C min^{-1}; 20 minute isothermal step at 100 °C (to ensure evaporation of the solvents); heat from 100 °C to 900 °C at a rate of 10 °C min.

All the FT-IR spectra were measured in the solid state on a PerkinElmer FT-IR Spectrometer Spectrum 100 with a universal ATR sampling accessory (diamond/ZnSe crystal). The spectra were recorded at 256 scans with a 4 cm^{-1} resolution.

Micro-Raman scattering measurements were carried out at room temperature in the backscattering geometry using RENISHAW 1000 micro-Raman system equipped with a CCD camera and a Leica microscope. An 1800 lines mm^{-1} grating was used for all measurements, providing a spectral resolution of ~ 1 cm^{-1}. As an excitation source the Ar^+ laser with 457 and 514 nm excitation lines and the He-Ne laser with 633 nm excitation with variable powers were used. Measurements were taken with 10 seconds of exposure time and 4 accumulations. The laser spot was focused on the sample surface using a 50x objective with short-focus working distance. Raman spectra were collected on numerous spots on the sample and recorded with Peltier cooled CCD camera. Only one spectrum was collected per spot. The intensity ratio I_D/I_G was obtained by taking the peak intensities after a baseline corrections. The data were collected and analyzed with Renishaw Wire and GRAMS software.

Raman mapping measurements were collected at room temperature using RENISHAW in-Via Raman system coupled with CCD camera. Samples were deposited on glass cover slides No 1. The laser spot was focused on the sample surface using a 100x oil immersion objective (N.A. = 1.4). As excitation source laser at 488 nm with 9 mW power was used. An 1800 lines mm^{-1} grating was used, providing a spectral resolution of ~ 1 cm^{-1}. Raman maps were taken with 0.2 seconds of exposure time, one accumulation and total number

of points 128x128. The data were collected and analyzed with Wire 3.1 software and NT-MDT Nova software.

The UV-Vis and the UV-Vis-NIR Absorption spectra were recorded on a Perkin Elmer UV/Vis Spectrometer Lambda 35 and a Perkin Elmer UV-Vis-NIR Spectrometer Lambda 1050 respectively. All the data were recorded after 1 cycle, with an interval of 1 nm, slit width of 2 nm and scan speed of 240 nm min^{-1}.

Samples were illuminated by using a portable UVP ultraviolet lamp equipped with a combination of shortwave (254 nm)/longwave (365 nm) and a Schott KL 1500 LCD Visible lamp (560-900 nm).

AFM topographic images were collected in semi-contact mode with an NT-MDT inverted configuration system. Silicon tips with reflectance gold coated on the back, tip apex radius 10 nm, force constant 2 N/m and frequency 170 kHz were used. The data were collected and analyzed with NT-MDT Nova software. Samples were prepared for analysis by dispersing the nanotubes in high purity DMF by sonication and spin coating on mica substrates.

3. Results and Discussion

3.1 Purification, oxidation and covalent functionalization of SWCNTs with Spiropyrans. Purified and oxidized (o-SWCNTs (**1**)) single walled carbon nanotubes were obtained by reaction of raw HiPco SWCNTs with nitric acid followed by a strong oxidation treatment with piranha solution using a reported protocol [21, 22] (Fig. 1).

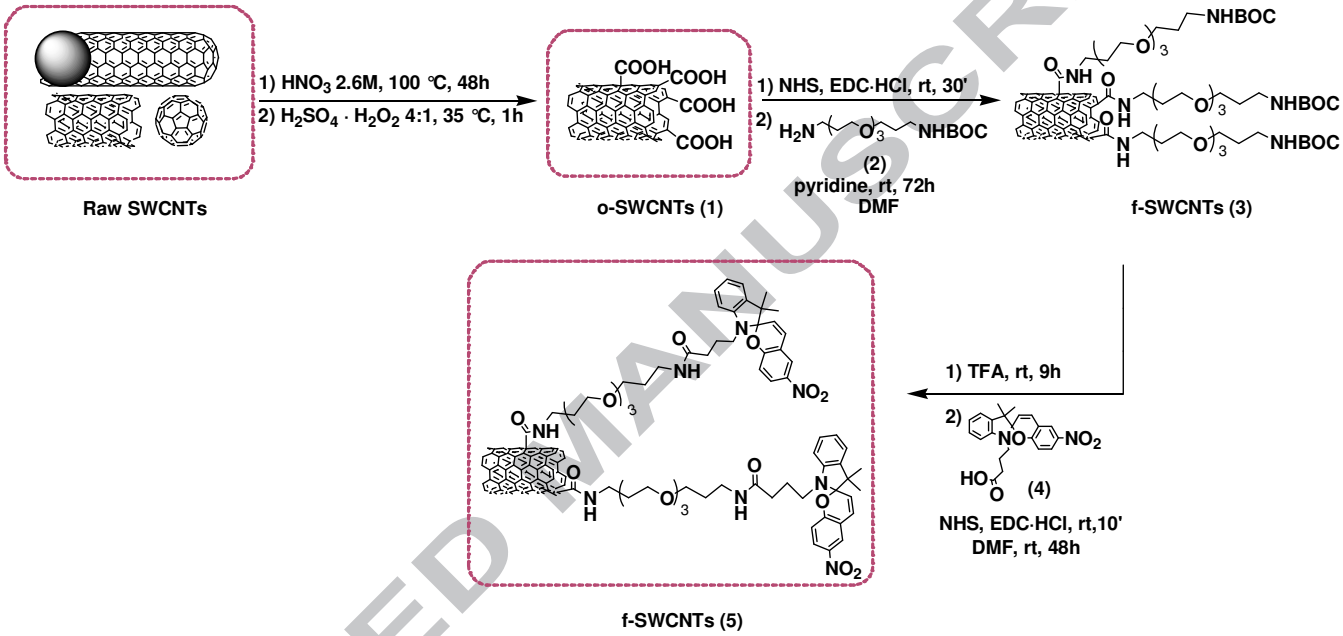

Fig. 1: Oxidation (o-SWCNTs (**1**)) and covalent functionalization of SWCNTs with spiropyran (f-SWCNTs (**5**)).

The purification step leads to the formation of open ends as well as defect sites on the SWCNTs surface. The oxidation step is applied to homogenize and reduce the dimensional dispersion of p-SWCNTs, and to obtain SWCNTs enriched with –COOH functional groups at the end caps which are the most reactive regions in the SWCNT structure [23-25]. The covalent functionalization of o-SWCNTs (**1**) was performed using

an amide coupling procedure in which an amine terminated short chain polyethylene glycol (PEG) linker was introduced onto the SWCNTs in order to increase the dispersibility. To ensure single ended chain attachment, one of the two amino groups was first protected using a tert-butoxycarbonyl (Boc) moiety (Fig. 1, (**2**)). Following removal of the Boc protecting group using triflouroacetic acid, spiropyran (**4**) was converted to an activated ester using NHS and EDC·HCl. A coupling procedure was again used to afford the spiropyran functionalized nanotubes f-SWCNTs (**5**). The number of amine groups that reacted with the SP derivatives was estimated at 59% by Kaiser test [26] (Fig. S1 in the S.I.).

3.2 Characterization of chemically modified SWCNTs. In order to provide a complete picture of the composition of the functionalized SWCNT we use different techniques such as thermal gravimetric analysis (TGA), Fourier transform infrared (FT-IR), Raman, UV-Vis-NIR absorbance spectroscopies and atomic force microscopy (AFM).

3.2.1 Thermogravimetric analysis. Thermogravimetric analysis has been used to evaluate the purity and degree of functionalization of the raw, oxidized (**1**) and functionalized SWCNTs (**5**) (Fig. 2 and S2). It should be noted that all non-reacted reagents were removed by careful washing after each chemical treatment. The TGA of the oxidized (**1**) and functionalized SWCNTs (**5**) performed in air show a weight loss of about 20% at 400 ºC and 30% at 450 ºC, respectively, as compared to about only 7% at 350 ºC of the raw SWCNTs. We assume that this weight loss occurring during fragmentation is due to pyrolysis of the hydrogenated carbon residues. On the basis of

this assumption, we estimated that the degree of functionalization is of one organic functional group every 15 and 116 carbon atoms respectively. In order to evaluate the amount of impurities present on the SWCNTs the residue remaining at 900 ºC was taken into account. It is reduced from 25% in the raw nanotubes to 0% in our functionalized samples, confirming the success of the purification procedure as shown in Figure 2B.

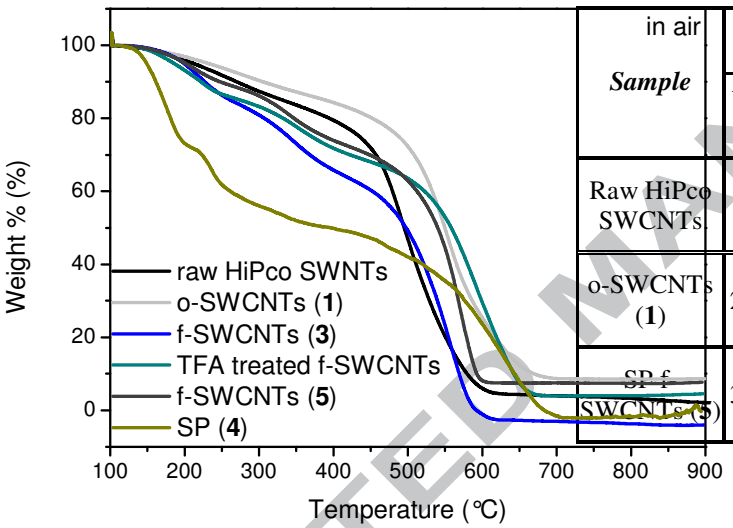

Sample	TGA in air		
	Weight loss %	*1 functional group every*	*residue % @ 900 °C*
Raw HiPco SWCNTs	7 at 350°C	-	24
o-SWCNTs (**1**)	20 at 400°C	15C	0
SP-f-SWCNTs (**5**)	30 at 450°C	116C	2

Fig. 2: Graph] TGA traces in air of raw and functionalized SWCNTs; Table] Weight losses, estimated number of carbon atoms per organic group and residue percentages for raw HiPco, oxidized (**1**) and spiropyran functionalized (**5**) SWCNTs.

To determine whether covalent functionalization was achieved the first derivative curves from the TGA analysis have been evaluated (Fig. 3A) focusing on the temperature

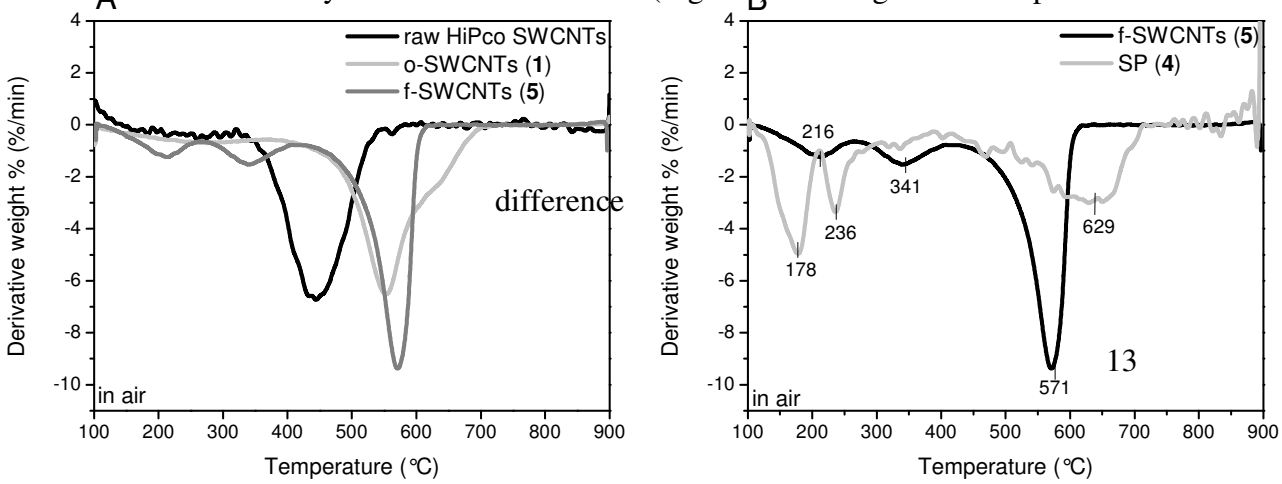

maxima between the raw HiPco SWCNTs, the o-SWCNTs (**1**) and the f-SWCNTs (**5**) below the graphitic decomposition temperatures.

Fig. 3: TGA first derivative traces of A] pristine SWCNTs, o-SWCNTs (**1**) and f-SWCNTs (**5**) B] f-SWCNTs (**5**) and spiropyran (**4**) recorded under air flow with a temperature increase of 10 °C min^{-1}.

TGA experiments were also performed on the pure SP (**4**), and Fig. 3B shows a comparison with that of the f-SWCNTs (**5**). It is evident that SP (**4**) is almost completely decomposed at 400 °C displaying two temperature maximum weight loss rates at 178 °C and 236 °C. These maxima also appear for the f-SWCNTs (**5**), although shifted to higher values of 215 °C and 341 °C, indicating the presence of SPs on the nanotube material.

3.2.2 FT-IR Spectroscopy. IR spectra of raw HiPco SWCNTs, o-SWCNTs (**1**) and f-SWCNTs (**5**) are illustrated in Fig. 4. The stretching vibrations observed between 1750 cm^{-1} and 1700 cm^{-1} are characteristic of the carboxyl group, and can be assigned to the oxygenated moieties introduced during the oxidative treatment of the SWCNTs. An additional indication of successful covalent functionalization is a decrease in

transmittance observed in the region 1700-650 cm^{-1} when comparing the o-SWCNTs (**1**) to the raw HiPco SWCNTs, as purification and doping processes introduce holes into the valence band of the SWCNTs that lead to an increase in the IR absorption bands (Fig. S3 in the S.I.)[5].

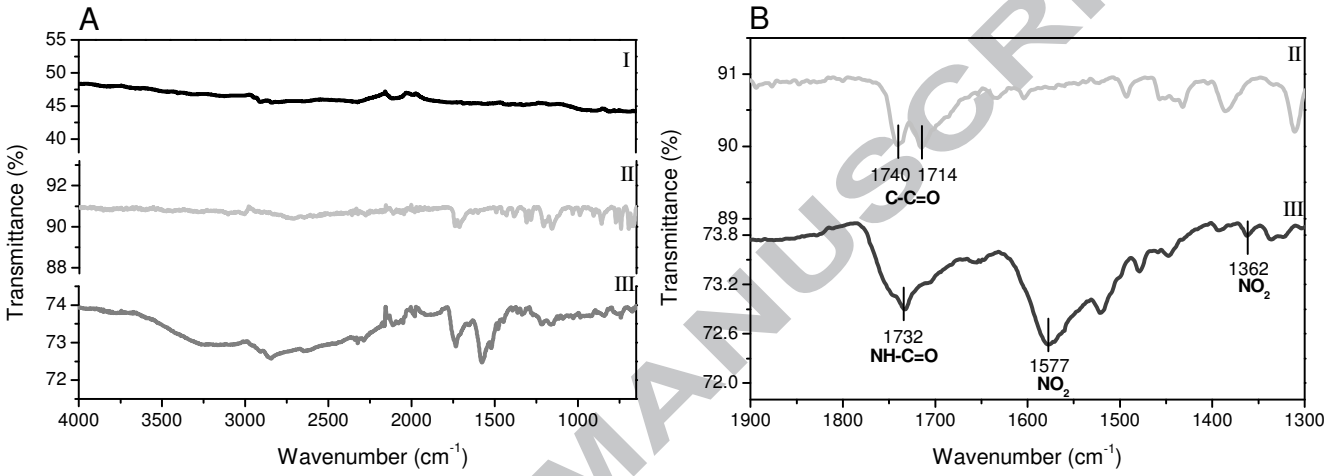

Fig. 4: A] FT-IR spectra of (I) raw HiPco SWCNTs, (II) o-SWCNTs (**1**) and (III) f-SWCNTs (**5**); B] Stretching vibrations assignment for (II) o-SWCNTs (**1**) and (III) f-SWCNTs (**5**). The peaks intensities are more than 3 times the peak to peak noise observed. To improve data visualization the spectra have been baseline corrected.

On comparison of the f-SWCNTs (**5**) spectrum with that of the oxidized material additional bands were observed indicating the presence of aliphatic chains, amidic, ether and amino groups (see Experimental). In addition the distinctive nitro absorption bands at

1577 and 1362 cm^{-1} are clearly evident (Fig. 4B III), indicating the presence of the spiropyran molecule on the material.

3.2.3 Micro-Raman Spectroscopy. The covalent functionalization of the SWCNTs [I_D/I_G ratios calculations] and the detection of spiropyran molecules attached to the tubes [functional groups shift assignment] were confirmed by performing Raman Spectroscopy analysis [27-29]. Micro-Raman scattering measurements were carried out on all samples at room temperature using three different excitation wavelengths (457, 514 and 633 nm) [8] in order to collect all the varying diameter contributions. Fig. 5 illustrates the Raman spectra of HiPco R0546, o-SWCNTs (**1**) and f-SWCNTs (**5**) using an excitation wavelength of 633 nm. (Additional Raman spectra are displayed in Fig. S4 in the S.I.).

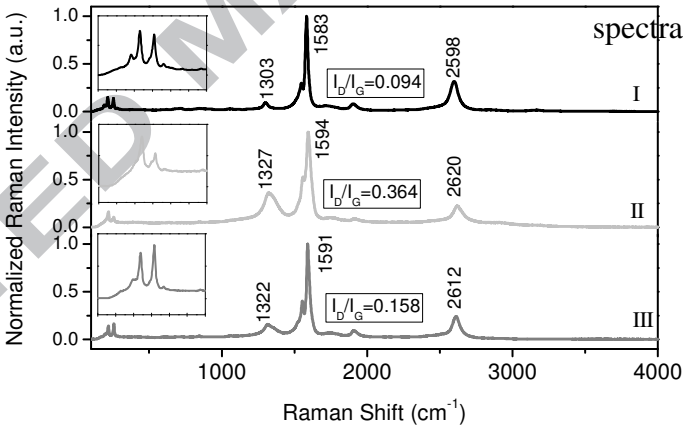

Fig. 5: Micro-Raman analyses (λ_{exc}= 633 nm) of (I) HiPco R0546, (II) o-SWCNTs (**1**) and (III) f-SWCNTs (**5**). In the insets the RBM analyses are reported.

The most significant spectral features observable are: 1) the radial breathing mode (RBM) band (100-400 cm^{-1}) that corresponds to the radial vibration of the carbon atoms in phase [30]; 2) the D-band (1300-1400 cm^{-1}), also called the "disorder" band, that is

related to the breathing motions of the sp^2 carbon atoms in rings and it can be activated by the presence of defects on the nanotube surface [31]; 3) the G-band (1500-1600 cm^{-1}), also called "tangential" mode, that consists of two subbands G^+ and G^- related to the axial and circumferential in plane vibrations respectively in semiconducting nanotubes [32]; 4) the 2D-band (2600-2800 cm^{-1}) which is the overtone of the D-band that is a fingerprint of the graphitic structure [33]. We took into consideration the I_D/I_G ratio as an indirect measure of the degree of functionalization [8, 23, 29].

It is clearly evident from Fig. 5 that the I_D/I_G ratio increases when comparing raw to oxidized nanotubes. This increase is indicative of the breakage of the graphene sheet symmetry that in the present case can be associated with the introduction of oxygenated functionalities onto the nanotube surface. From the result reported we can thus assume that the covalent functionalization of the SWCNTs was indeed successful. Conversely, however comparing o-SWCNTs (**1**) and f-SWCNTs (**5**) a decrease in the I_D/I_G ratio is observed. This is most likely due to removal of the carboxylated carbonaceous fragments (CCFs) [34, 35] during chemical treatment and the subsequent stringent washing procedure employing a range of organic solvents.

3.2.4 Raman mapping. Raman mapping measurements were performed at room temperature on the SP f-SWCNTs (**5**) (Fig. 6).

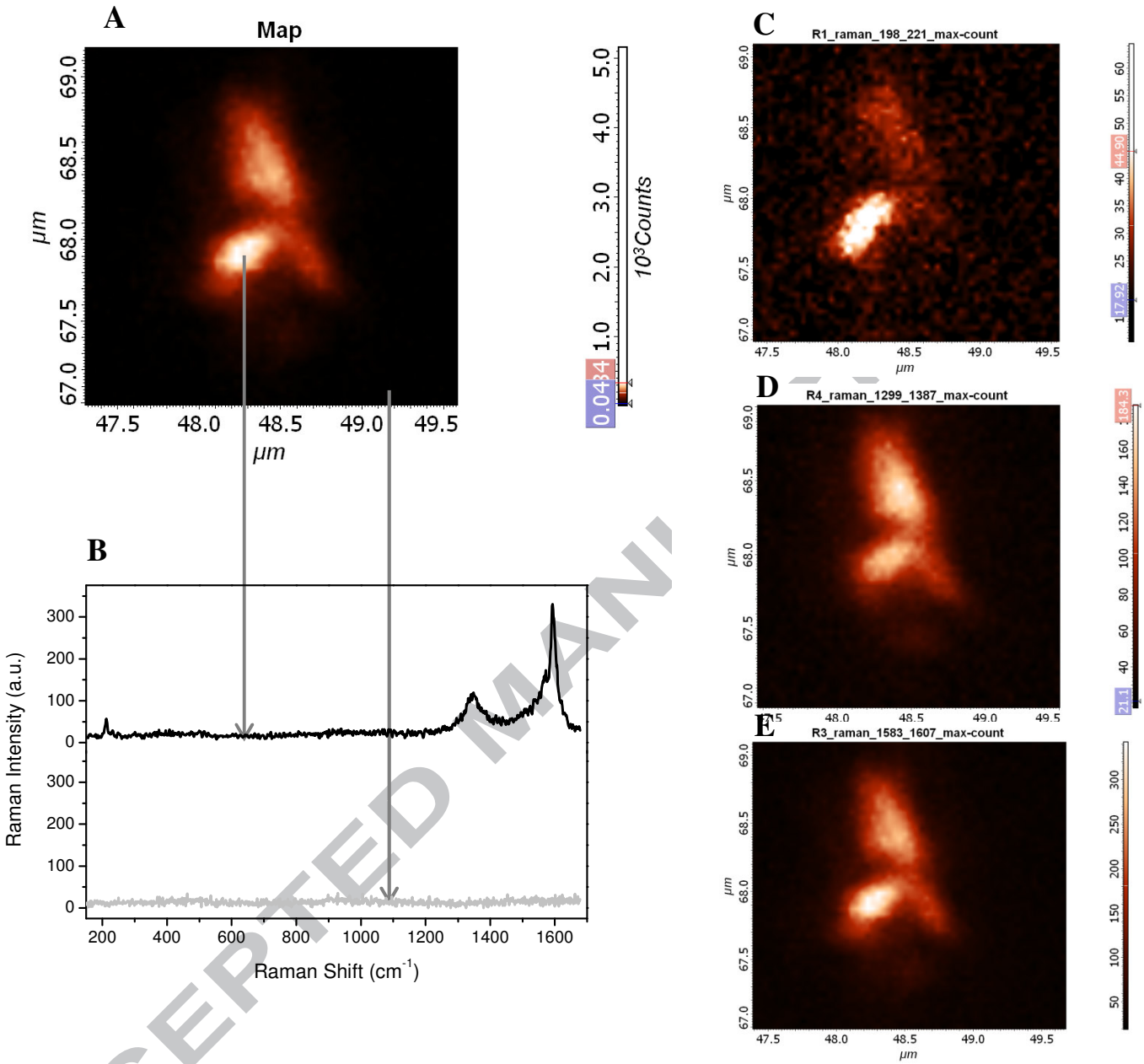

Fig. 6: Raman mapping analysis (λ_{exc}= 488 nm) of f-SWCNTs (**5**). A] Full map image, B] single Raman spectra from the region marked in the full Raman map, C] RBM mapping in the range 198-221 cm^{-1}, D] D-band mapping, E] G-band mapping. Time exposure 0.2 sec, one accumulation, point number 128 x 128.

The presence of functionalities bound to the tubes was confirmed after single Raman measurements with high exposure time in the different mapped areas. Some typical vibrations of the functional groups introduced on the tubes were recorded in the range from 300 to 1100 cm^{-1} and are reported in Fig. 7.

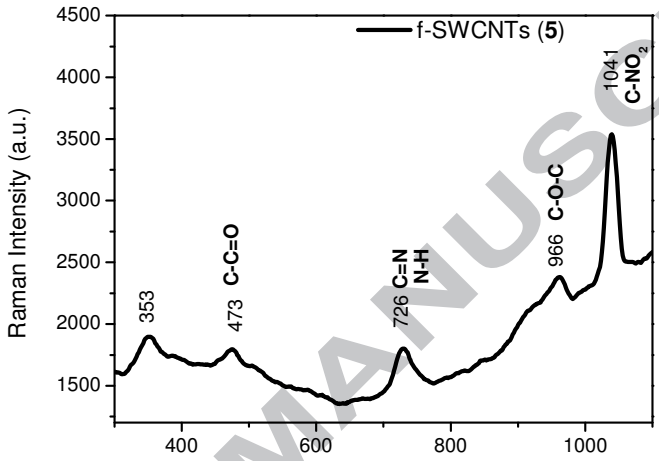

Fig. 7: Micro-Raman analysis (λ_{exc}= 488 nm) of f-SWCNTs (**5**) in the functional group region.

Raman shifts assigned to stretching and deformation vibrations of amidic groups (473, 726 cm^{-1}), stretching vibrations of ethers linkages (966 cm^{-1}) and nitro aromatic groups (1041 cm^{-1}) ensure that the PEG chain and the spiropyran derivative have been effectively introduced onto nanotube surface.

3.2.5 Atomic Force Microscopy. AFM analyses were performed in order to estimate nanotube dimensions. f-SWCNTs (**5**) were dispersed in DMF via sonication and subsequently spin-coated onto freshly cleaned mica substrates. Fig. 8 illustrates a

typically dispersed individual f-SWCNT on the substrate surface, with diameter and length of approximately 1 nm and 600 nm, respectively.

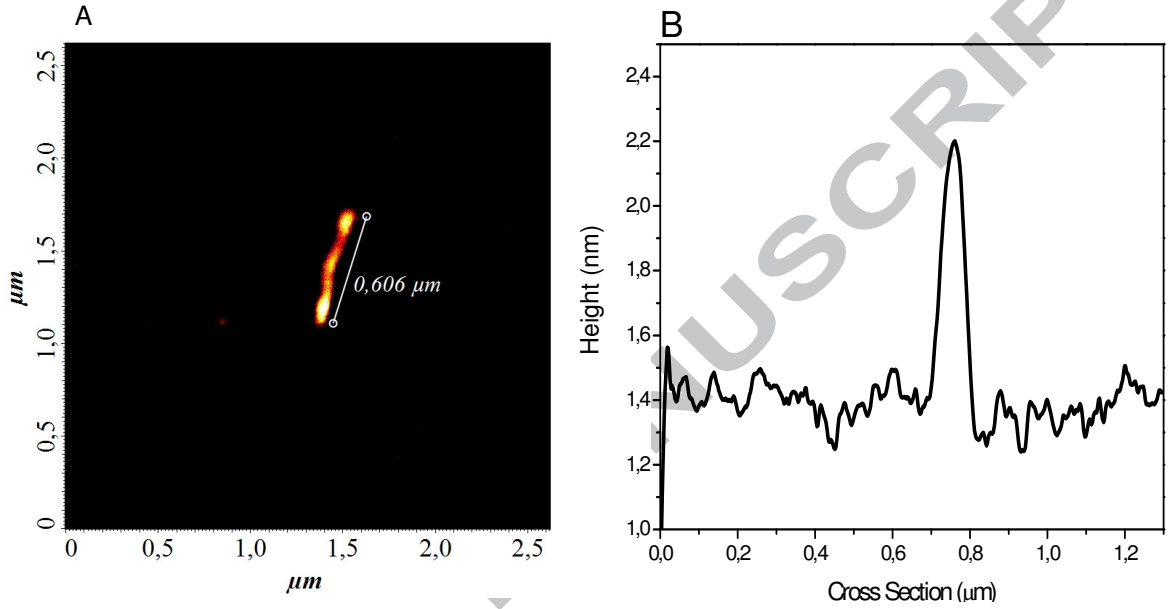

Fig. 8: AFM topographic image of A] an individual SP f-SWCNTs (**5**) B] cross-section profile illustrating the height of the nanotube.

3.2.6 UV-Vis-NIR Absorbance Spectroscopy. Optical absorption spectroscopy have been used to evaluate the successful covalent functionalization of the nanotubes by analysis of the electronic structure changes [5, 36]. UV-Vis-NIR absorption spectra of

nanotubes after nitric acid purification step, oxidation (**1**) and functionalization (**5**) recorded on the supernatant of a centrifuged sample of nanotubes (10^{-2} mg/mL) dispersed in DMF are reported in Fig. S5. We found that the electronic structure of the SWCNTs is perturbed following chemical modification of the purified tubes and the loss in number and intensity of the van Hove transitions is indicative of the effective oxidation of the tubes [36, 37].

3.3 On-off switching of SWCNTs functionalized with spiropyran molecules. In order to observe the switching of the f-SWCNT (**5**) construct we first studied the optical changes which could be induced on molecular SP in solution upon UV irradiation and storage in the dark. A reversible reaction between the spiropyran (**6**) and merocyanine (ME) is observable upon irradiation with UV light (365 nm) and subsequent storage in the dark. The absorption spectra are reported in Fig. S6 in the S.I. where it can be seen that after 30 seconds of UV irradiation, the absorption band of the merocyanine (at 594 nm) increases in intensity and after 8 minutes of storage in the dark it returns to its initial value.

On comparison of the UV-Vis absorption spectra of the o-SWCNTs (**1**) and f-SWCNTs (**5**) a peak is clearly observable at 417 nm in the latter, corresponding to the bound spiropyran (**6**) (Fig. S7 in the S.I.). This absorption band is shifted with respect to molecular spiropyran (**6**) in solution, which is regarded as stemming from π–π interactions between the spiropyran and the graphitic nanotube surface. This is similar to shifts reported for merocyanines bound to bulk materials [38].

The photoresponsiveness of f-SWCNTs (**5**) in solution was demonstrated by measuring the optical changes that occurred after UV and Vis light irradiations. Fig. 9A illustrates the nature of such changes before and after UV illumination.

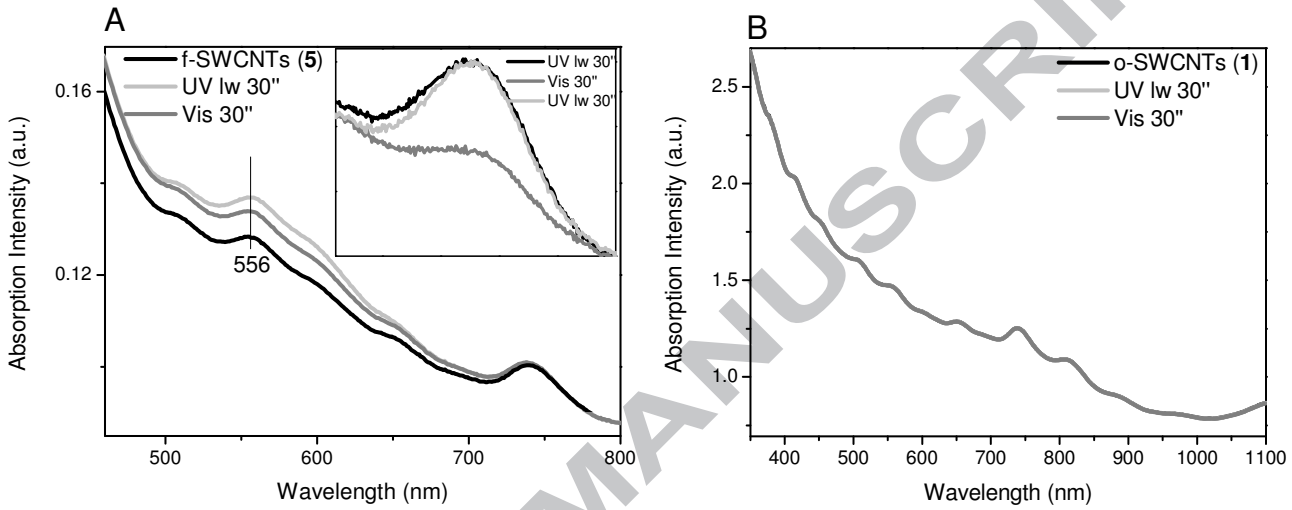

Fig. 9: A] f-SWCNTs (**5**) response to UV (365 nm) and Vis (560-900 nm) illumination for 30 seconds. In the inset difference absorption spectra of f-SWCNTs (**5**) after 30 seconds UV, Vis and UV illuminations; B] UV-Vis absorption spectra of o-SWCNTs (**1**) collected on the supernatant of initial 0.1 mg/mL nanotubes in DMF after 30 seconds UV illumination (365 nm) and 30 seconds Vis illumination (560-900 nm).

As a result of UV irradiation (365 nm) an increase in absorbance in the region characteristic to the merocyanine isomer was recorded. It was demonstrated that the merocyanine absorption band at 556 nm switched back to the starting value following 30

seconds of illumination with visible light (560-900 nm) as illustrated in Fig. 9A. For improved data visualization, absorption spectra of f-SWCNTs (**5**) were subtracted from the spectra recorded after UV and Vis illumination, as reported in the inset in Fig. 9A. The same experiments performed on oxidized nanotubes (**1**), showed no photoresponsiveness as displayed in Fig. 9B. The reversible switching of the spiro molecule is demonstrated schematically in Fig. 10A and the changes in the absorbance band intensity of SP f-SWCNTs (**5**) are reproducible and the on-off switching cycles are reported in Fig. 10B.

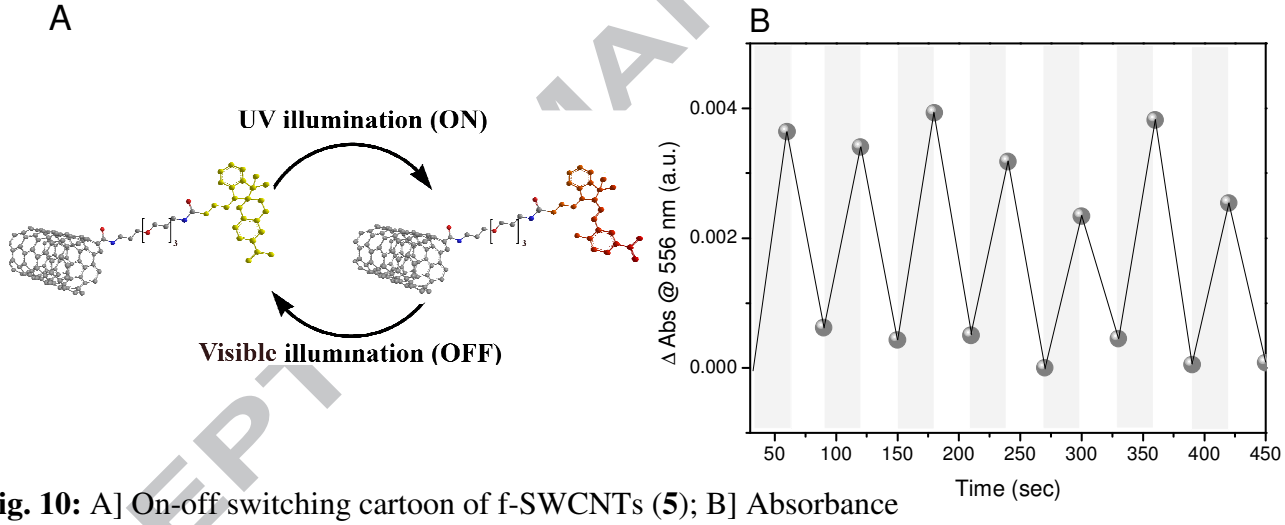

Fig. 10: A] On-off switching cartoon of f-SWCNTs (**5**); B] Absorbance changes at 556 nm of f-SWCNTs (**5**) solutions following UV (365 nm) and visible (560-900 nm) illumination cycles. Gray and white bars indicate the UV and the Vis irradiation respectively. The spectra were collected on the supernatant of initial 0.1 mg/mL nanotubes in DMF.

4. Conclusions

We have demonstrated the preparation of spiropyran functionalized SWCNTs. All stages of the synthetic process have been characterized by means of TGA, AFM, FT-IR and Raman Spectroscopies to obtain a comprehensive overview of their structural, electronic and chemical properties. TGA analysis was used to demonstrate that the residue remaining following complete pyrolysis decreased from 24% in the raw nanotubes to 0% in the functionalized samples, confirming purification of the nanomaterial. Weight losses calculated from TGA analyses suggested the presence of a high degree of functionalization of the tubes, estimated at approximately about one organic functional group every 116 carbon atoms. The analyses of the first derivative curves ensured that the SP moieties were present in the functionalized sample. The presence of aliphatic chains, amidic, ether and amino groups are confirmed by the stretching vibrations observed in the FT-IR spectrum of f-SWCNTs as well as the nitro group present on the spiropyran aromatic ring. Topographic atomic force microscopy showed that the nanotube lengths were approximately 600 nm. Raman Spectroscopy has been determinant in indirectly confirming the covalent functionalization of the SWCNTs; the I_D/I_G ratio increases when comparing raw to chemically modified SWCNTs. Micro Raman measurements have been performed on all nanotube samples with three different laser excitation wavelengths (457, 514 and 633 nm) in order to examine all diameter/chirality contributions. The photoresponsiveness of our f-SWCNTs in solution was demonstrated by measuring the optical changes that occurred after UV and Vis light illuminations. UV irradiation resulted in a substantial increase of the band at 556 nm and Vis light irradiation induced restoration of the initial intensity. We report light induced

reversible conversion of spiropyran molecules attached to the SWCNT from the close spiro conformation to the open merocyanine form.

Acknowledgments

This work was supported by Science Foundation Ireland (PIYRA 07/YI2/I1052). The authors wish to thank Dr. Manuel Ruther, Dr. Paula Colavita and the support of IRCSET and Intel (Postgraduate Research Scholarships to EDC) and Trinity College Dublin (Trinity Award to MN).

Supplementary data. Supplementary data associated with this article can be found in the online version.

Captions to Figures

Fig. 1: Oxidation (o-SWNTs (**1**)) and covalent functionalization of SWNTs with spiropyran (f-SWNTs (**5**)).

Fig. 2: A] TGA traces in air of raw and functionalized SWCNTs; B] Weight losses, estimated number of carbon atoms per organic group and residue percentages for raw HiPco, oxidized (**1**) and spiropyran functionalized (**5**) SWCNTs.

Fig. 3: TGA first derivative traces of A] pristine SWNTs, o-SWNTs (**1**) and f-SWNTs (**5**) B] SP f-SWNTs (**5**) and pure spiropyran (**4**) recorded under air flow with a temperature increase of 10 °C min^{-1}.

Fig. 4: A] FT-IR spectra of (I) raw HiPco SWNTs, (II) o-SWNTs (**1**) and (III) f-SWNTs (**5**); B] Stretching vibrations assignment for (II) o-SWNTs (**1**) and (III) f-SWNTs (**5**). The peaks intensities are more than 3 times the peak to peak noise observed. To improve data visualization the spectra have been baseline corrected.

Fig. 5: Micro-Raman analyses (λ_{exc}= 633 nm) of (I) HiPco R0546, (II) o-SWNTs (**1**) and (III) f-SWNTs (**5**). In the insets the RBM analyses are reported.

Fig. 6: Raman mapping analysis (λ_{exc}= 488 nm) of f-SWNTs (**5**). A] Full map image, B] single Raman spectra from the region marked in the full Raman map, C] RBM mapping in the range 198-221 cm^{-1}, D] D-band mapping, E] G-band mapping. Time exposure 0.2 sec, one accumulation, point number 128x128.

Fig. 7: Micro-Raman analysis (λ_{exc}= 488 nm) of f-SWNTs (**5**) in the functional group region.

Fig. 8: AFM topographic image of A] an individual SP f-SWNTs (**5**) B] cross-section profile illustrating the height of the nanotube.

Fig. 9: A] f-SWNTs (**5**) response to UV (365 nm) and Vis (560-900 nm) illumination for 30 seconds. In the inset difference absorption spectra of f-

SWNTs (**5**) after 30 seconds UV, Vis and UV illuminations; B] UV-Vis absorption spectra of o-SWNTs (**1**) collected on the supernatant of initial 10^{-1} mg/mL nanotubes in DMF after 30 seconds UV illumination (365 nm) and 30 seconds Vis illumination (560-900 nm).

Fig. 10: A] On-off switching cartoon of f-SWNTs (**5**); B] Absorbance changes at 556 nm of f-SWNTs (**5**) solutions following UV (365 nm) and visible (560-900 nm) illumination cycles. Gray and white bars indicate the UV and the Vis irradiation respectively. The spectra were collected on the supernatant of initial 10^{-1} mg/mL nanotubes in DMF.

References

[1] Iijima S. Helical Microtubules of Graphitic Carbon. Nature 1991;354(6348):56-8.

[2] Iijima S, Ichihashi T. Single-Shell Carbon Nanotubes of 1-nm diameter. Nature 1993;363(6430):603-5.

[3] Niyogi S, Hamon MA, Hu H, Zhao B, Bhowmik P, Sen R, et al. Chemistry of single-walled carbon nanotubes. Acc Chem Res 2002;35(12):1105-13.

[4] Burghard M. Electronic and vibrational properties of chemically modified single-wall carbon nanotubes. Surf Sci Rep 2005;58(1-4):1-109.

[5] Itkis ME, Niyogi S, Meng ME, Hamon MA, Hu H, Haddon RC. Spectroscopic study of the Fermi level electronic structure of single-walled carbon nanotubes. Nano Lett 2002;2(2):155-9.

[6] Hasan T, Sun Z, Wang F, Bonaccorso F, Tan PH, Rozhin AG, et al. Nanotube-Polymer Composites for Ultrafast Photonics. Adv Mater 2009;21(38-39):3874-99.

[7] Dyke CA, Tour JM. Overcoming the insolubility of carbon nanotubes through high degrees of sidewall functionalization. Chem Eur J 2004;10(4):813-7.

[8] Singh P, Campidelli S, Giordani S, Bonifazi D, Bianco A, Prato M. Organic functionalisation and characterisation of single-walled carbon nanotubes. Chem Soc Rev 2009;38:2214-30.

[9] Raymo FM, Giordani S. All-optical processing with molecular switches. Proc Natl Acad Sci U.S.A. 2002;99(8):4941-4.

[10] Raymo FM, Giordani S. Signal processing at the molecular level. J Am Chem Soc 2001;123(19):4651-2.

[11] Ren JQ, Tian H. Thermally stable merocyanine form of photochromic spiropyran with aluminum ion as a reversible photo-driven sensor in aqueous solution. Sensors 2007;7(12):3166-78.

[12] Natali M, Soldi L, Giordani S. A reversible Zn(II) selective spiropyran-based receptor. Tetrahedron 2010.

[13] Kawata S, Kawata Y. Three-dimensional optical data storage using photochromic materials. Chem Rev 2000;100(5):1777-88.

[14] Hirshberg Y. Reversible Formation and Eradication of Colors by Irradiation at Low Temperatures. A Photochemical Memory Model. J Am Chem Soc 1956;78:2304-12.

[15] de Silva AP, Vance TP, West MES, Wright GD. Bright molecules with sense, logic, numeracy and utility. Org Biomol Chem 2008;6(14):2468-80.

[16] Khairutdinov RF, Itkis ME, Haddon RC. Light modulation of electronic transitions in semiconducting single wall carbon nanotubes. Nano Lett 2004;4(8):1529-33.

[17] Guo XF, Small JP, Klare JE, Wang YL, Purewal MS, Tam IW, et al. Covalently bridging gaps in single-walled carbon nanotubes with conducting molecules. Science 2006;311(5759):356-9.

[18] Guo XF, Huang LM, O'Brien S, Kim P, Nuckolls C. Directing and sensing changes in molecular conformation on individual carbon nanotube field effect transistors. J Am Chem Soc 2005;127:15045-7.

[19] Yildiz I, Deniz E, Raymo FM. Fluorescence modulation with photochromic switches in nanostructured constructs. Chem Soc Rev 2009;38(7):1859-67.

[20] Aakeroy CB, Hurley EP, Desper J, Natali M, Dowglawi A, Giordani S. The balance between closed and open forms of spiropyrans in the solid state. Cryst Eng Comm 2010;DOI: 10.1039/b914566d.

[21] Giordani S, Colomer JF, Cattaruzza F, Alfonsi J, Meneghetti M, Prato M, et al. Multifunctional hybrid materials composed of [60]fullerene-based functionalized-single-walled carbon nanotubes. Carbon 2009;49:578-88.

[22] Movia D, Del Canto E, Giordani S. Spectroscopy of single-walled carbon nanotubes in aqueous surfactant dispersion. Phys Stat Sol B 2009;246(11-12):2704-07.

[23] Hamon MA, Itkis ME, Niyogi S, Alvaraez T, Kuper C, Menon M, et al. Effect of rehybridization on the electronic structure of single-walled carbon nanotubes. J Am Chem Soc 2001;123(45):11292-3.

[24] Haddon RC. Chemistry of the Fullerenes - The manifestation of strain in a class of continuous aromatic-molecules. Science 1993;261(5128):1545-50.

[25] Haddon RC. Rehybridization and pi-orbital overlap in nonplanar conjugated organic-molecules-pi-orbital axis vector (POAV) analysis and 3-dimetional huckel molecular-orbital (3D-HMO) theory. J Am Chem Soc 1987;109(6):1676-85.

[26] Kaiser E, Colescot RL, Bossinge CD, Cook PI. Color test for the detection of free terminal amino groups in solid-phase synthesis of peptides. Anal Biochem 1970;34(2):595-8.

[27] Landi BJ, Cress CD, Evans CM, Raffaelle RP. Thermal oxidation profiling of single-walled carbon nanotubes. Chem Mater 2005;17(26):6819-34.

[28] Costa S, Borowiak-Palen E, Kruszynska M, Bachmatiuk A, Kalenczuk RJ. Characterization of carbon nanotubes by Raman spectroscopy. Materials Sci-Poland 2008;26(2):433-41.

[29] Graupner R. Raman spectroscopy of covalently functionalized single-wall carbon nanotubes. J Raman Spectrosc 2007;38(6):673-83.

[30] Rao AM, Richter E, Bandow S, Chase B, Eklund PC, Williams KA, et al. Diameter-selective Raman scattering from vibrational modes in carbon nanotubes. Science 1997;275(5297):187-91.

[31] Ferrari AC, Robertson J. Interpretation of Raman spectra of disordered and amorphous carbon. Phys Rev B 2000;61(20):14095-107.

[32] Lazzeri M, Piscanec S, Mauri F, Ferrari AC, Robertson J. Phonon linewidths and electron-phonon coupling in graphite and nanotubes. Phys Rev B 2006;73:155426

[33] Ferrari AC. Raman spectroscopy of graphene and graphite: Disorder, electron-phonon coupling, doping and nonadiabatic effects. Solid State Commun 2007;143(1-2):47-57.

[34] Salzmann CG, Llewellyn SA, Tobias G, Ward MAH, Huh Y, Green MLH. The Role of Carboxylated Carbonaceous Fragments in the Functionalization and Spectroscopy of a Single-Walled Carbon-Nanotube Material. Adv Mater 2007;19:883-7.

[35] Shao L, Tobias G, Salzmann CG, Ballesteros B, Hong SY, Crossley A, et al. Removal of amorphous carbon for the efficient sidewall functionalisation of single-walled carbon nanotubes. Chem Commun 2007:5090-2.

[36] Chen J, Hamon MA, Hu H, Chen YS, Rao AM, Eklund PC, et al. Solution properties of single-walled carbon nanotubes. Science 1998;282(5386):95-8.

[37] Liu X, Pichler T, Knupfer M, Fink J. Electronic properties of FeCl3-intercalated single-wall carbon nanotubes. Phys Rev B 2004;70:205405.

[38] Sayama K, Hara K, Ohga Y, Shinpou A, Suga S, Arakawa H. Significant effects of the distance between the cyanine dye skeleton and the semiconductor surface on the photoelectrochemical properties of dye-sensitized porous semiconductor electrodes. New J of Chem 2001;25:200-2.